Size-effect of oligomeric cholesteric liquid-crystal microlenses on the optical specifications

Chloé Bayon, Gonzague Agez, Michel Mitov

▶ **To cite this version:**

Chloé Bayon, Gonzague Agez, Michel Mitov. Size-effect of oligomeric cholesteric liquid-crystal microlenses on the optical specifications. Optics Letters, 2015, 40 (20), pp.4763–4766. 10.1364/OL.40.004763 . hal-01730530

HAL Id: hal-01730530
https://hal.science/hal-01730530

Submitted on 13 Mar 2018

HAL is a multi-disciplinary open access archive for the deposit and dissemination of scientific research documents, whether they are published or not. The documents may come from teaching and research institutions in France or abroad, or from public or private research centers.

L'archive ouverte pluridisciplinaire **HAL**, est destinée au dépôt et à la diffusion de documents scientifiques de niveau recherche, publiés ou non, émanant des établissements d'enseignement et de recherche français ou étrangers, des laboratoires publics ou privés.

Optics Letters

Size-effect of oligomeric cholesteric liquid-crystal microlenses on the optical specifications

Chloé Bayon, Gonzague Agez, and Michel Mitov*

Centre d'Elaboration de Matériaux et d'Etudes Structurales (CEMES), CNRS, University Paul-Sabatier, 29 rue J. Marvig, F-31055 Toulouse cedex 4, France
**Corresponding author: mitov@cemes.fr*

Received 21 August 2015; revised 21 September 2015; accepted 21 September 2015; posted 23 September 2015 (Doc. ID 247553); published 13 October 2015

In cholesteric liquid-crystalline microlenses, we have studied the role of the microlens size on the focused light intensity and the focal length. We have found that the intensity is maximized by aiming a specific range for the diameter and the thickness of microlenses and that the focal length is adjusted by controlling the diameter and the annealing time of the optical film. Cholesteric microlenses may be used as wavelength-tunable directional light sources in organic soft-matter circuits. © 2015 Optical Society of America

OCIS codes: (230.3720) Liquid-crystal devices; (350.3950) Micro-optics; (080.3620) Lens system design; (080.3630) Lenses; (070.6120) Spatial light modulators.

http://dx.doi.org/10.1364/OL.40.004763

Liquid crystal (LC)-based microlenses [1] gain benefit from: the self-organization property of LCs; their anisotropic structure; the tuning of the focal length, readily reached by setting the material parameters or by applying an electrical voltage; and the compactness, the flexibility, and the easy-to-implement fabrication schemes that LCs offer for the realization of optical organic films.

Cholesteric LC (CLC) microlenses have recently appeared [2,3]. Rod-like chiral molecules of a CLC adopt a mesoscopic helical structure, which gives rise to the fundamental property of selective light reflection in the Bragg band [4,5]. To provide the focusing effect and to perform the beam shaping, CLC microlenses rely on the intrinsic chiral organization of CLC and not on the shape of the lens, as is usually the case. They require the formation of polygonal textures that exist in an array of contiguous polygonal cells. Each cell behaves like a microlens [2].

Polygonal textures may be observed in flat CLC films when the helical axis is strongly tilted with respect to the substrates [6]. Recent investigations [2,7–10] have focused on the optical and structural properties of polygonal textures found in oligomeric CLCs (polysiloxanes with achiral and chiral mesogens as side chains) [11]. The flat film is in hybrid conditions, i.e., the molecules are parallel to the solid interface (glass plate) and perpendicular to the air interface. After quenching below the glass-transition temperature (~50°C), the helical structure and the color properties are stored inside a solid film ready to be handled at room temperature. The structure and the light transmission properties of microlenses were characterized in 3D, and it was shown that their focusing properties—as a spot or as a "donut"—were wavelength tunable [2].

In this Letter, first we characterize the geometry of CLC microlenses and then we show how parameters of paramount importance, such as the focal length and the light intensity, behave with the microlens size.

CLC oligomers from Wacker Chemie GmbH were used. The CLC phase appears between 180°C–210°C (clearing temperature range) and 40°C–50°C (glass-transition temperature range). The chemical formula is given in [12]. The molecule consists of a siloxane cyclic chain to which two types of side chains are attached via aliphatic spacers: an achiral mesogen and a chiral cholesterol-bearing mesogen. The molar percentage of chiral mesogen can vary from 31% [in the case of silicon red (SR)] to 50% [in the case of silicon blue (SB)]. The pitch of the helical structure and therefore the reflection wavelength depend on the SB:SR proportion. We blended SB and SR compounds at 40:60 wt. %; thus the mean position of the reflection band is located in the middle of the visible spectrum (560 nm). The transmittance spectrum of the sample was published in [7]. The cholesteric structure is left-handed. The ordinary and extraordinary refractive indices are assessed to be $n_0 = 1.4$ and $n_e = 1.6$ [13]. The birefringence is 0.2. The helical pitch is 370 nm.

Open flat films of varying thicknesses are coated at 140°C on a plain glass plate. (The thickness is monitored with calibrated spacers placed between glass plates. The upper plate is then removed after quenching, when the film is solid. Afterward, the thickness is checked by using a micrometer screw gauge.) The annealing of the viscous film occurs at 140°C for 5 h; the time corresponds to the formation of an array of microlenses with an optimized focal point (clear-cut shape and maximum transmitted intensity). The film is then promptly quenched at room temperature.

The spontaneous nucleation and growth of the polygonal texture gives rise to an array of polygons with various sizes, as shown in Fig. 1(a), when the film thickness is equal to 12.5 μm. To draw the peculiar space tessellation that leads to the formation of self-organized polygonal cells, we use a Voronoï diagram

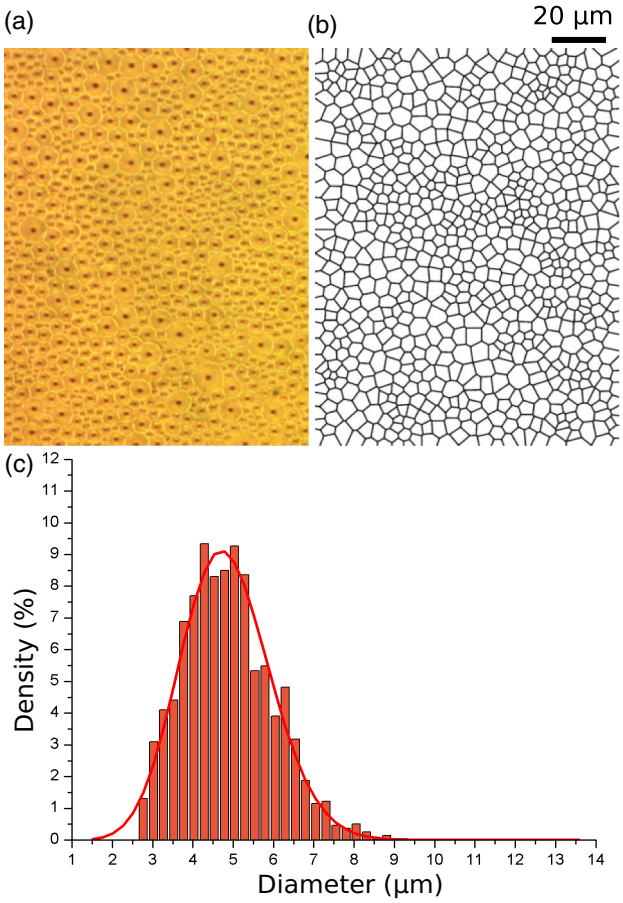

Fig. 1. Self-organized array of microlenses: texture and size distribution. Film thickness = 12.5 µm. (a) Optical micrograph of the polygonal texture (transmission mode, unpolarized light). Each cell corresponds to a microlens. (b) Voronoï diagram. (c) Histogram and Poisson size distribution of polygonal cells. The diameter of the circle inscribed into a cell is chosen to describe the microlens size.

[Fig. 1(b)], which is useful for modeling various natural patterns [14]. We generate it by using Fortune's algorithm [15] from a set of points that are the optical centers of cells [black spots in Fig. 1(a)]. To characterize the size distribution of cells, we have chosen the diameter of the circle that is inscribed into the polygonal cell. The histogram in Fig. 1(c) is obtained by using the Granulometry plugin implemented in ImageJ software. The diameter ranges from 2.7 to 8.5 µm with a mean value close to 5.0 µm. Polygons with larger diameters, up to 35 µm (not shown here), may be exceptionally observed.

The variation of the microlens diameter when the thickness varies from 3.0 to 50.0 µm is displayed in Fig. 2. We deduce from the Poisson distributions that the mean diameter increases from 4.3 to 5.7 µm when the thickness increases up to 50 µm. The formation of polygons comes from the propagation of distortions in the orientation of the helix axis below the free surface because of hybrid anchoring conditions [7]. This frustration is progressively released when the thickness increases, which could explain the increase of the mean diameter in the same time. A fine control of the lateral size of the lens is thus made possible by varying the film thickness.

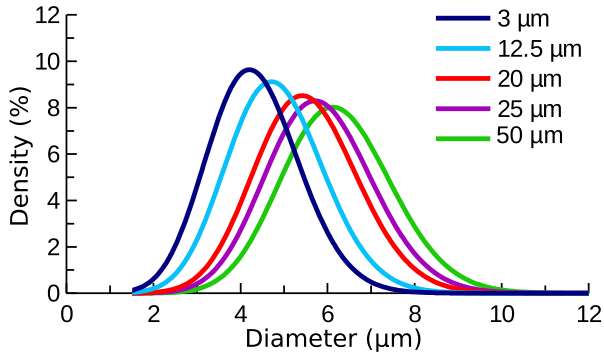

Fig. 2. Poisson distribution of the microlens mean diameter for different film thicknesses.

We used a spectrometer equipped with a standard confocal microscope (XploRA from Horiba) to scan the layer over the area of a single polygon at room temperature. A 3 mm diameter circular hole is placed above the halogen light source of the microscope and at a distance of 8 cm below the layer in order to approximate a point source. The transmission baseline is recorded through the substrate (glass plate) without any extra material. In an XY transmission map, each pixel is related to a transmittance spectrum. The scanning area of a map is 14.5 µm × 14.5 µm with a step of 0.5 µm. An XY map is then related to a stack of 841 (29 × 29) spectra. The images are magnified by a factor of 10, and a bicubic interpolation is used.

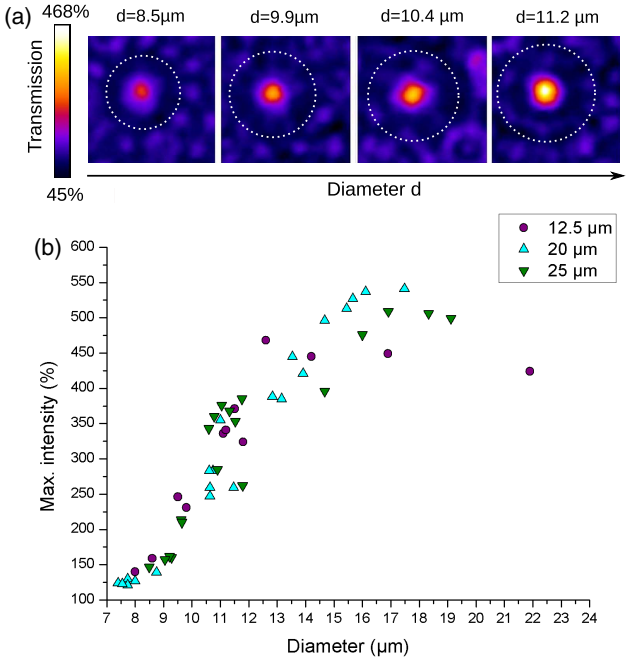

Fig. 3. (a) Mapping of the light transmitted in the band edge (500–550 nm) for polygons of varying diameter. Film thickness = 12.5 µm. The dashed circles depict the lens-polygon size. The scale is the same for all the maps and ranges from 45% to 468%. (Because the light is differently concentrated on the polygon surface, the transmission scale per unit area can reach values above 100%.) The images are magnified by a factor of 10, and a bicubic interpolation is used. (b) Maximum transmitted intensity versus diameter for various film thicknesses.

The XY maps shown in Fig. 3 have been recorded at a Z height for which the central transmittance is maximum, i.e., in the focal plane. The mapping of the transmitted light for polygons with varying diameter is investigated in the so-named band edge (500–550 nm) in which the focalized intensity is maximum.

In this section devoted to the optical behavior of polygonal microlenses, we define their diameter from optical criteria as follows. The polygonal texture is observed by reflection and unpolarized light. The borders of each polygonal cell are brilliant and smooth. A circle fitting at the best of these borders is traced. Its diameter is defined as the microlens diameter and chosen as the descriptor for the presentation of results. The diameter dependence of the maximum intensity transmitted through a microlens is displayed in Fig. 3. First, the intensity of the focus point increases with the polygon size as a consequence of a larger area for the light collection. Then, saturation appears above a threshold diameter. This threshold depends on the film thickness and increases with it. The thicker the film is, the longer the light–matter interaction path is, and the light collection is enhanced.

The fact that the optical layer is a 3D-organized film in an LC state ensures the full continuity of the global architecture. Two adjacent polygons are continuously connected without defects. This unique property minimizes undesired diffraction due to the lens edges and optimizes the fill factor. The optical film is not composed of a collection of shaped items on a specific substrate but is the result of a tailoring of the structure within the single layer.

The same investigation in the Bragg band (470–500 nm) leads to a similar behavior. In the red band (700–800 nm), the size of the donut (where the intensity is focused) and the central spot (for which the light is off) also increase with the polygon diameter.

As a parameter of paramount importance, the tunability of the focal length with the polygon size is investigated in Fig. 4. Interestingly, the variation is linear for a large set of diameters from 8.5 to 32 μm. Inside this range, the effective back focal length $f_{E,b}$ measured from the bottom of the film, as defined by ISO 14880-1, may be adjusted from 0 to −160 μm. This dependence of the focal length with the diameter can explain the saturation of the focus point intensity. Indeed, larger the diameter is, larger the area of light collection is. In return a longer

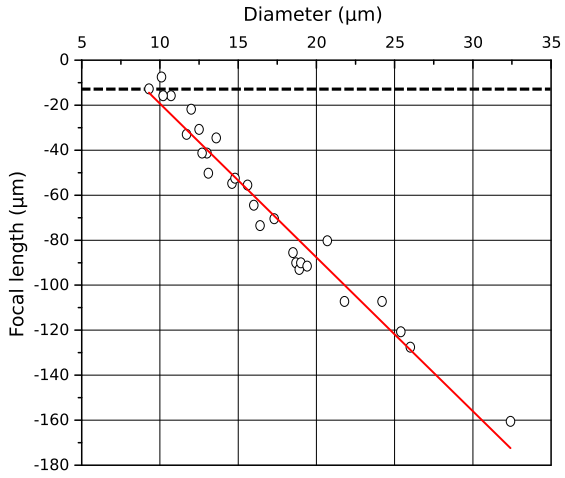

Fig. 4. Focal length versus diameter. Film thickness = 12.5 μm. The dotted line corresponds to the bottom of the film.

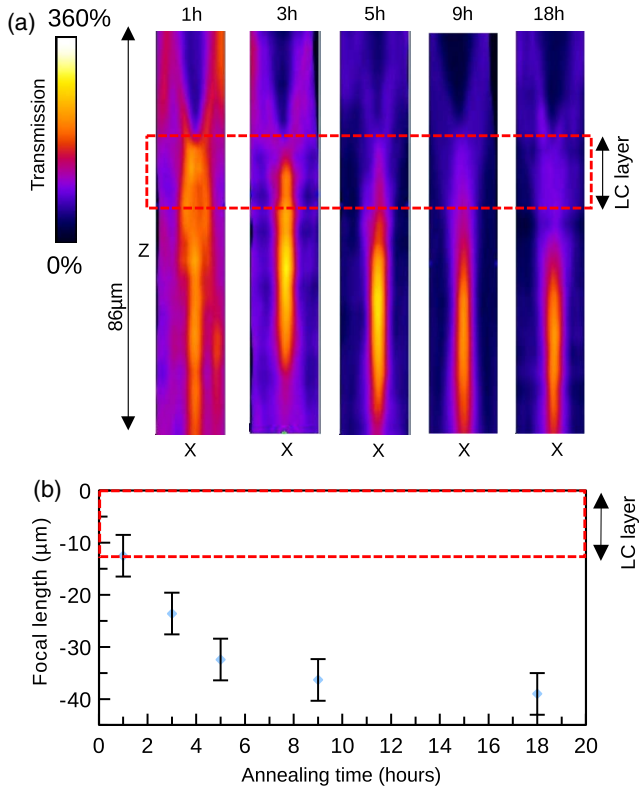

Fig. 5. Behavior of the focusing properties of a microlens with the annealing time. Film thickness = 12.5 μm. (a) Cross-sectional mapping of the transmitted light in the band edge (500–550 nm) for different annealing times. The images are magnified by a factor of 10, and a bicubic interpolation is used. (b) Focal length versus annealing time.

focal length implies a weaker light concentration. The diameter for which the intensity is maximized is a compromise between a large area—to collect more light—and a reasonable focal length that effectively concentrates the light. Measurements show that the most favorable balance is reached for a diameter in the 13–18 μm range, depending on the film thickness.

The behavior of the focusing with the annealing time is investigated in Fig. 5. When the annealing (at fixed temperature) occurs, the bulk structure reorganizes with time: the orientation of the helical axis changes as a consequence of the adaptation of the CLC organization to hybrid anchoring conditions. The XZ vertical cross sections are built from a stack of XY images recorded at different Z heights with a step equal to 4 μm. These cross sections are thus not a temporal representation of light propagation, for which the light before the layer would be the incident plane wave. The intensity below the layer depicts the intensity distribution in the virtual part of the image space. The focal length increases with the annealing time, which constitutes a control parameter to adjust it easily. This dependence demonstrates that the lens effect is directly related to the cholesteric structure and not to a lens curvature nor an index gradient.

The microlens behavior with a circularly or linearly polarized incident light was reported in the Supplementary Information of Ref. [2].

In conclusion, we have characterized the focal length and the maximum transmitted intensity of CLC microlenses in relation

to their geometry (lateral size and thickness). A peculiar lens diameter has to be targeted when specific transmission properties are desired. This objective may be aimed by adjusting the film thickness. The focal length is set by controlling two parameters: the lens diameter and the annealing time. The lens properties are obtained by using a complete self-assembly process. The fabrication method is versatile because it does not require a surface-modified substrate, which may be a flat or curved glass plate or a sheet of rollable plastic.

In the present set of results, the lens size exhibits a distribution. For some applications, a controlled monodisperse distribution could be desired. When required, methods leading to the formation of a polygonal texture with a single-size diameter may be developed by coating the CLC film onto a patterned [16,17] or surface-relief [18] substrate. The nucleation of polygons would be forced in specific defect sites (like metallic or polymeric dots). When these sites are lithographed or printed at periodic distances, the lateral growth of polygons, and so their size, may be controlled.

Related applications of chiral LC microlenses are in the field of wavelength-tunable chiro-optical devices and lab-on-a-chip optical systems that offer the combined benefits of multiple light manipulation capabilities, seamless integration, and mechanical stability.

Acknowledgment. The authors thank Dr. E. Hanelt from Wacker-Chemie GmbH (Munich, Germany) for providing them with oligomers and constant support.

REFERENCES

1. S. Xu, Y. Li, Y. Liu, J. Sun, H. Ren, and S.-T. Wu, Micromachines **5**, 300 (2014).
2. C. Bayon, G. Agez, and M. Mitov, Lab Chip **14**, 2063 (2014).
3. S. Pleasants, Nat. Photonics **8**, 505 (2014).
4. H. Kelker and R. Hatz, *Handbook of Liquid Crystals* (Verlag Chemie, 1980), pp. 293–337.
5. M. Mitov, Adv. Mater. **24**, 6260 (2012).
6. Y. Bouligand, J. Phys. **33**, 715 (1972).
7. G. Agez, R. Bitar, and M. Mitov, Soft Matter **7**, 2841 (2011).
8. A. Bobrovsky, K. Mochalov, A. Chistyakov, V. Oleinikov, and V. Shibaev, Macromol. Chem. Phys. **213**, 2639 (2012).
9. A. Bobrovsky, O. Sinitsyna, A. Abramchuk, I. Yaminsky, and V. Shibaev, Phys. Rev. E **87**, 012503 (2013).
10. O. Sinitsyna, A. Bobrovsky, I. Yaminsky, and V. Shibaev, Colloid Polym. Sci. **292**, 1567 (2014).
11. F.-H. Kreuzer, N. Häberle, H. Leigeber, R. Maurer, J. Stohrer, and J. Weis, *Organosilicon Chemistry Set: From Molecules to Materials*, N. Auner and J. Weis, eds. (Wiley-VCH Verlag GmbH, 2005), pp. 566–586.
12. G. Agez and M. Mitov, J. Phys. Chem. B **115**, 6421 (2011).
13. D. C. Zografopoulos, E. E. Kriezis, M. Mitov, and C. Binet, Phys. Rev. E **73**, 061701 (2006).
14. J.-S. Ferenc and Z. Néda, Phys. A **385**, 518 (2007).
15. M. de Berg, M. van Kreveld, M. Overmars, and O. Schwarzkopf, *Computational Geometry*, 2nd revised ed. (Springer-Verlag, 2000), pp. 151–160.
16. H. Ren, Y.-H. Fan, and S.-T. Wu, Opt. Lett. **29**, 1608 (2004).
17. H. T. Dai, Y. J. Liu, X. W. Sun, and D. Luo, Opt. Lett. **17**, 4317 (2009).
18. J.-H. Na, S. C. Park, S.-U. Kim, Y. Choi, and S.-D. Lee, Opt. Express **20**, 864 (2012).

193.44.32.45 {ts '2018-03-13 08:43:30'}